The mitochondrial thioredoxin reductase system (TrxR2) in vascular endothelium controls peroxynitrite levels and tissue integrity

Petra Kameritsch[a,1], Miriam Singer[a,1], Christoph Nuernbergk[a,1], Natalia Rios[b,c], Aníbal M. Reyes[b,c], Kjestine Schmidt[d,e], Julian Kirsch[a], Holger Schneider[a], Susanna Müller[f], Kristin Pogoda[a], Ruicen Cui[a], Thomas Kirchner[f], Cor de Wit[d,e], Bärbel Lange-Sperandio[g], Ulrich Pohl[a,h], Marcus Conrad[i,j], Rafael Radi[b,c,2], and Heike Beck[a,h,2]

[a]Walter Brendel Centre of Experimental Medicine, Biomedical Center Munich, Ludwig-Maximilians-University, 82152 Planegg, Germany; [b]Departamento de Bioquímica, Facultad de Medicina, Universidad de la República, 11800 Montevideo, Uruguay; [c]Centro de Investigaciones Biomédicas, Facultad de Medicina, Universidad de la República, 11800 Montevideo, Uruguay; [d]Institute of Physiology, University of Lübeck, 23562 Lübeck, Germany; [e]Partner Site Hamburg/Kiel/Lübeck, German Centre for Cardiovascular Research, 23562 Lübeck, Germany; [f]Institute of Pathology, Ludwig Maximilians-University, 80337 Munich, Germany; [g]Department of Pediatrics, Dr. v. Hauner Children's Hospital, Ludwig-Maximilians-University, 80337 Munich, Germany; [h]German Centre for Cardiovascular Research, Munich Heart Alliance, 80802 Munich, Germany; [i]Institute of Metabolism and Cell Death, Helmholtz Zentrum München, 85764 Neuherberg, Germany; and [j]Laboratory of Experimental Oncology, National Research Medical University, Moscow 117997, Russia

Contributed by Rafael Radi, December 4, 2020 (sent for review December 16, 2019; reviewed by Mark B. Hampton and Santiago Lamas)

The mitochondrial thioredoxin/peroxiredoxin system encompasses NADPH, thioredoxin reductase 2 (TrxR2), thioredoxin 2, and peroxiredoxins 3 and 5 (Prx3 and Prx5) and is crucial to regulate cell redox homeostasis via the efficient catabolism of peroxides (TrxR2 and *Trxrd2* refer to the mitochondrial thioredoxin reductase protein and gene, respectively). Here, we report that endothelial TrxR2 controls both the steady-state concentration of peroxynitrite, the product of the reaction of superoxide radical and nitric oxide, and the integrity of the vascular system. Mice with endothelial deletion of the *Trxrd2* gene develop increased vascular stiffness and hypertrophy of the vascular wall. Furthermore, they suffer from renal abnormalities, including thickening of the Bowman's capsule, glomerulosclerosis, and functional alterations. Mechanistically, we show that loss of *Trxrd2* results in enhanced peroxynitrite steady-state levels in both vascular endothelial cells and vessels by using a highly sensitive redox probe, fluoresceinboronate. High steady-state peroxynitrite levels were further found to coincide with elevated protein tyrosine nitration in renal tissue and a substantial change of the redox state of Prx3 toward the oxidized protein, even though glutaredoxin 2 (Grx2) expression increased in parallel. Additional studies using a mitochondria-specific fluorescence probe (MitoPY1) in vessels revealed that enhanced peroxynitrite levels are indeed generated in mitochondria. Treatment with Mn(III)tetrakis(1-methyl-4-pyridyl)porphyrin [Mn(III)TMPyP], a peroxynitrite-decomposition catalyst, blunted intravascular formation of peroxynitrite. Our data provide compelling evidence for a yet-unrecognized role of TrxR2 in balancing the nitric oxide/peroxynitrite ratio in endothelial cells in vivo and thus establish a link between enhanced mitochondrial peroxynitrite and disruption of vascular integrity.

thioredoxin reductase | nitric oxide | peroxynitrite | mitochondria | redox

Selenocysteine-containing mitochondrial thioredoxin reductase (TrxR2) is the key regulator of the thioredoxin system and essential for mitochondrial redox homeostasis (1–3). This system constitutes a primary defense against peroxides produced in mitochondria, such as hydrogen peroxide and peroxynitrite (4). TrxR2 is necessary for maintaining thioredoxin 2 (Trx2) in its reduced state by using electrons from NADPH. In turn, Trx2 is a cofactor of mitochondrially localized peroxiredoxin 3 (Prx3) and peroxiredoxin 5 (Prx5) that reduce H_2O_2 and peroxynitrite* generated by mitochondrial metabolism (1, 2, 4–7). The reaction rate constants of H_2O_2 and peroxynitrite with the fast reacting thiols of both Prx3 and Prx5 have been compiled recently (4). Notably, Prx3, the only peroxiredoxin which is exclusively localized in mitochondria (8, 9)†, was reported to accept electrons also from glutaredoxin 2 (Grx2) (10). Among the biologically recognized functions, TrxR2 plays essential roles in hematopoiesis, heart development, and heart function (11, 12). In a previous study, we could show that loss of TrxR2 in endothelial cells (ECs) attenuated vascular remodeling processes following ischemic events and led to a prothrombotic and proinflammatory endothelium (13). While these studies pointed

Significance

Vascular oxidative stress and endothelial cell dysfunction contribute to various human pathologies. Here, we show that, in vascular endothelial cells, a key mitochondrial antioxidant enzyme, namely thioredoxin reductase 2 (TrxR2), plays a central role in the control of vascular integrity. Its targeted loss is associated with disruption of both nitric oxide (·NO) and redox homeostasis in vivo. Impaired TrxR2 activity leads to elevated steady-state levels of peroxynitrite, reflecting the decreased bioavailability of ·NO by its $O_2^{\cdot-}$ mediated oxidative inactivation. Thus, TrxR2 represents a central control point of peroxynitrite levels by providing reducing equivalents to mitochondrial peroxiredoxins that, in turn, catalytically reduce peroxynitrite to nitrite. The data additionally support pharmacological approaches for mitochondrial peroxynitrite detoxification under conditions of vascular oxidative stress.

Author contributions: N.R., A.M.R., K.S., T.K., C.d.W., B.L.-S., U.P., M.C., R.R., and H.B. designed research; P.K., M.S., C.N., N.R., A.M.R., K.S., J.K., H.S., S.M., K.P., R.C., and B.L.-S. performed research; N.R. and R.R. contributed new reagents/analytic tools; P.K., M.S., A.M.R., K.S., J.K., H.S., S.M., K.P., R.C., C.d.W., B.L.-S., R.R., and H.B. analyzed data; and M.C., R.R., and H.B. wrote the paper.

Reviewers: M.B.H., University of Otago; and S.L., Centro de Biología Molecular Severo Ochoa.

The authors declare no competing interest.

[1]P.K., M.S., and C.N. contributed equally to this work.

[2]To whom correspondence may be addressed. Email: rradi@fmed.edu.uy or Heike.Beck@med.uni-muenchen.de.

This article contains supporting information online at https://www.pnas.org/lookup/suppl/doi:10.1073/pnas.1921828118/-/DCSupplemental.

Published February 12, 2021.

*Peroxynitrite refers to the sum of peroxynitrite anion ($ONOO^-$) and peroxynitrous acid (ONOOH) ($pK_a = 6.8$). The actual reactant with the fast reacting thiol of the peroxiredoxins is ONOOH.

†In human cells, Prx5 is located in mitochondria, peroxisomes, the cytosol, and the nucleus.

toward an important role of TrxR2 in the cardiovascular system, the underlying biochemical mechanisms, particularly in vivo, have remained largely unclear. Unlike many other cell types in the body, ECs are unique as they are constantly exposed to changing biochemical and mechanical stimuli. Furthermore, they do not just separate the circulating blood and the vascular smooth muscle cells but also have to fulfill a wide range of physiological tasks, including regulation of vascular tone, cellular adhesion, thromboresistance, smooth muscle cell proliferation, and inflammoresistance (14, 15). One of the most significant biomolecules that is involved in vascular endothelial function is the free radical nitric oxide (·NO) (16, 17). ·NO is not only an important vasodilator but also has antiinflammatory properties by inhibiting the synthesis and expression of cytokines and adhesion molecules that attract inflammatory cells and facilitate their entrance into the vessel wall (18, 19). Furthermore, ·NO suppresses platelet aggregation (20), vascular smooth muscle cell migration, and proliferation (21). Consequentially, a decreased synthesis of ·NO, as well as an enhanced inactivation, can result in endothelial dysfunction (22–24). Oxidative stress contributes to this phenomenon, starting with the diffusion-controlled reaction of ·NO with superoxide radical ($O_2^{\cdot-}$), which shortens the biological half-life and compromises the signaling actions of ·NO (25–28). In addition, the oxidative inactivation of ·NO by $O_2^{\cdot-}$ yields a powerful oxidizing and nitrating species, peroxynitrite anion (28, 29). Moreover, peroxynitrite itself leads to uncoupling of endothelial nitric oxide synthase to become a dysfunctional $O_2^{\cdot-}$ and peroxynitrite-producing enzyme that additionally contributes to cellular oxidative stress (30, 31). A sustained overload of $O_2^{\cdot-}$ and, peroxynitrite combined with insufficient levels of ·NO may contribute to a switch of the endothelium from the quiescent stage toward an activated one, setting up a vicious cycle, causing endothelial dysfunction and inflammation. ECs are equipped with a number of antioxidant systems known to be potentially protective against vascular oxidative stress that, however, under persistent pathological stimuli, may become overwhelmed.

In this context, it is increasingly recognized that mitochondrial-derived $O_2^{\cdot-}$ and the disruption of mitochondrial redox homeostasis contribute to alter the signaling actions of ·NO in vascular biology (32–34). Besides the mitochondrial thioredoxin system, a number of professional redox systems, including mitochondrial superoxide dismutase (MnSOD/SOD2), glutathione peroxidase, and glutathione reductase, are involved in maintaining mitochondrial redox homeostasis.

However, the specific roles of these enzymes in the context of endothelial dysfunction are far from being understood. The fact that genetically modified mouse models revealed that many of the different antioxidant enzymes are indispensable for murine development (35–38) impedes further insights into their role for vascular homeostasis, and, to our knowledge, only a limited number of EC-specific transgenic mice have yet been described in this context (39–42). Interestingly, Trx2 transgenic mice that overexpress Trx2 specifically in the endothelium demonstrated an increased ·NO bioavailability and EC function, decreased oxidative stress, and reduced propensity to atheroma formation (3, 43).

The aim of this study was to analyze the impact of endothelial TrxR2 on vascular homeostasis (in vitro, ex vivo, and in vivo), focusing on its role on mitochondrial peroxynitrite catabolism. The data support that enhanced mitochondrial steady-state levels of peroxynitrite in vascular ECs are connected with disruption of redox homeostasis and vascular structural and functional integrity.

Results

Phenotypic Characterization of *Trxrd2*^{iECKO} Mice. Although, after knockout induction, the general appearance of tamoxifen-inducible endothelial cell-specific knockout mice (*Trxrd2*^{iECKO}) mice (KO) was inconspicuous compared to control animals (*Trxrd2*^{control}, WT), histological analysis revealed vascular alterations in many organs. Because the phenotypic changes were most pronounced in the kidney, we focused on this organ but also analyzed vessels in other tissues: e.g., skeletal muscle (Fig. 1 *A* and *B*), cremaster muscle (*SI Appendix*, Fig. S2 *A* and *B*), mesentery (Figs. 1 *C* and *D* and 5*A*), and aorta (*SI Appendix*, Fig. S3).

Arterial Wall Hypertrophy in *Trxrd2*^{iECKO} Mice. Analysis of the wall thickness and wall area of skeletal muscle arterioles, as well as of small renal arteries, revealed a statistically significant increase of both parameters in *Trxrd2*^{iECKO} mice (Fig. 1 *A* and *B*). The vessel luminal diameters (skeletal muscle arterioles, *Trxrd2*^{control}: 18.7 ± 0.8 vs. *Trxrd2*^{iECKO}: 19.1 ± 0.8 μm; small renal arteries, *Trxrd2*^{control}: 78.2 ± 6.2 vs. *Trxrd2*^{iECKO}: 92.1 ± 6.69 μm; $n = 5$ animals per group) were not different among the groups.

Blood Pressure Measurements and Increased Vascular Stiffness in Trxrd2^{iECKO} Mice. Arterial blood pressure was measured invasively in 10 control mice and 8 *Trxrd2*^{iECKO} mice. In both genotypes, arterial pressure and heart rate were higher during nighttime than daytime, indicating a circadian rhythm with higher locomotor activity during the nighttime period. During daytime, as well as during nighttime, systolic, mean, and diastolic pressure, as well as heart rate, were not different between *Trxrd2*^{control} and *Trxrd2*^{iECKO} mice (averaged [day 4, 6, 8, and 10] blood pressure values for *Trxrd2*^{control} mice [systolic/diastolic in mmHg]: 127.2 ± 3.1/96.4 ± 2.3 [daytime]; 138.7 ± 3.2/105 ± 2 [nighttime]; averaged heart rate per minute [day 4, 6, 8, and 10] 555 ± 13 [daytime], 588 ± 9 [nighttime]. *Trxrd2*^{iECKO} mice [systolic/diastolic in mmHg] daytime: 128.4 ± 5.6/95.4 ± 3.7; nighttime: 141.7 ± 6.6/106 ± 4.1; heart rate per minute daytime: 543 ± 10; nighttime: 600 ± 7) (*SI Appendix*, Fig. S1). Because analysis of data from the Framingham heart study revealed that arterial stiffness actually precedes the development of arterial hypertension (44), we cannulated freshly isolated mesenteric arteries from mice of both genotypes and determined stress–strain curves. Mesenteric arteries from *Trxrd2*^{iECKO} mice displayed a decreased passive distensibility, as indicated by a left-shift of the stress–strain curve when compared to *Trxrd2*^{control} mice (Fig. 1*C*). Consequently, the stiffness coefficient was significantly increased in *Trxrd2*^{iECKO} arteries (Fig. 1*D*). Decreased arterial compliance suggests structural remodeling of the arterial wall in *Trxrd2*^{iECKO} mice.

Intravital Microscopy Demonstrates an Impaired Response of Arterioles toward Vasodilatory Compounds in *Trxrd2*^{iECKO} Mice. To further analyze the impact of a deletion of TrxR2 on endothelial function, we studied arterioles in the cremaster muscle of six *Trxrd2*^{iECKO} (64 arterioles) and of six *Trxrd2*^{control} mice (58 arterioles). The arterioles exhibited maximal diameters ranging from 22 to 54 μm and were not different between genotypes (mean 37 ± 1 μm in both genotypes). The arterioles exhibited a spontaneous tone at rest amounting to 46 ± 2% of their maximal diameter in controls, and tone was similar in *Trxrd2*^{iECKO} mice (49 ± 2%). The endothelium dependent dilator acetylcholine (Ach) (0.1 to 10 μM) induced concentration-dependent dilations in both genotypes, but these dilations were significantly reduced in *Trxrd2*^{iECKO} at higher concentrations (*SI Appendix*, Fig. S2*A*). Likewise, the ·NO donor sodium nitroprusside (SNP) (0.1 to 10 μM) dilated arterioles in a concentration-dependent manner in both genotypes, but again with significantly less efficacy in *Trxrd2*^{iECKO} mice (*SI Appendix*, Fig. S2*B*).

Renal Capillary Density and Renal EC Morphology Are Impaired in *Trxrd2*^{iECKO} Mice. Since small renal arteries displayed an increase in vessel wall thickness, we tested whether EC loss of *Trxrd2* would affect kidney morphology and renal function. First, we

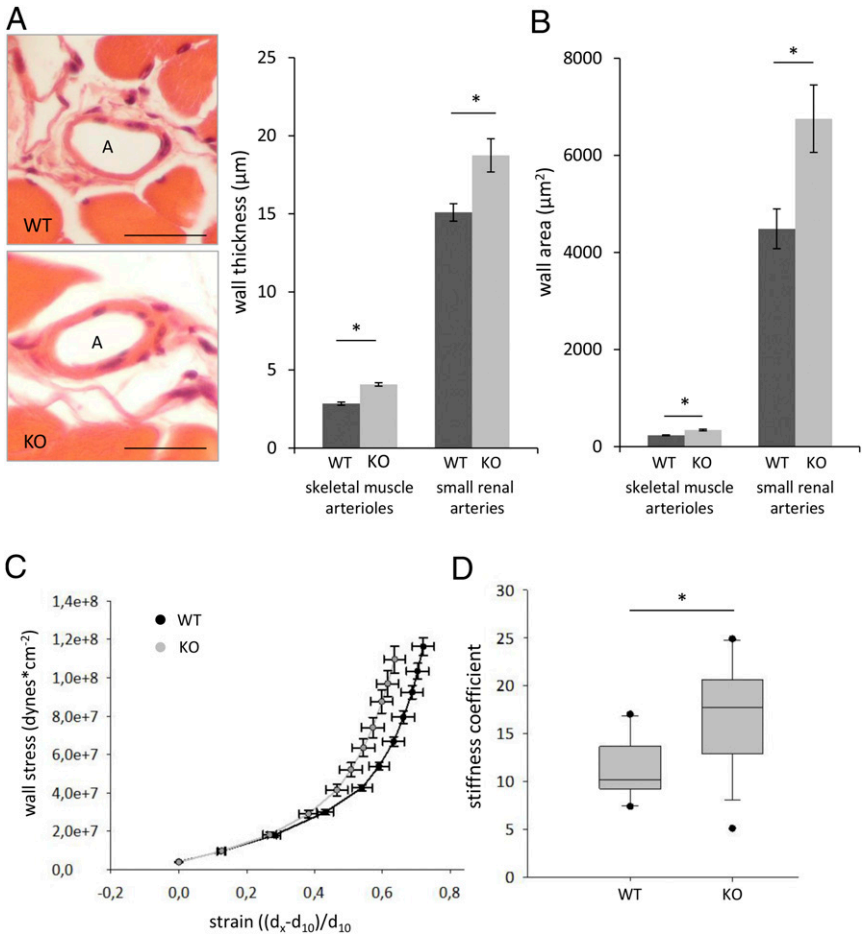

Fig. 1. Arterial wall hypertrophy and increased vascular stiffness in *Trxrd2*^{iECKO} mice. (*A*) The wall thickness of skeletal muscle arterioles (exemplified on the *Left*), as well as of small renal arteries, is significantly enhanced in *Trxrd2*^{iECKO} mice. (*B*) The wall area (µm^2) of skeletal muscle arterioles, as well as of small renal arteries, is significantly increased in *Trxrd2*^{iECKO} mice. (*A* and *B*) $n = 5$ animals per group, Mann–Whitney rank-sum test for skeletal muscle arterioles, *t* test for small renal arteries. A, arteriole. (Scale bar: 25 µm.) (*C*) Mesenteric arteries derived from *Trxrd2*^{iECKO} mice display a decreased passive distensibility, as indicated by a left-shift of the stress–strain curve when compared to wild-type animals. (*D*) The stiffness coefficient is significantly increased in *Trxrd2*^{iECKO} mice arteries (*C* and *D*: $n = 14$ vessels derived from four wild-type mice, and $n = 14$ vessels derived from five knockout mice, *t* test). *$P < 0.05$.

analyzed vascular density by measuring the CD-31–positive areas in glomeruli-containing tissue, as well as tubulointerstitial tissue. Interestingly, capillary density was significantly reduced in *Trxrd2*^{iECKO} mice within the glomeruli-containing area (Fig. 2*A*), but not within the tubulointerstitium (*Trxrd2*^{control}: 2.7% ± 0.2 vs. *Trxrd2*^{iECKO}: 2.2% ± 0.2; $n = 7$ animals per group). By periodic acid Schiff (PAS) staining, we could frequently observe enlargements of the capillary space of glomeruli (exemplified by Fig. 2*B*). Ultrastructural analysis further substantiated pathological endothelial changes by illustrating detachment of ECs from the glomerular basement membrane (Fig. 2*C*). Although the vascular alterations were most pronounced in the renal compartment, the phenotypic changes were not limited to the kidneys but were also detectable in other organs of *Trxrd2*^{iECKO} mice (the detachment of aortic ECs from the basal membrane is exemplified by *SI Appendix*, Fig. S3).

Thickening of the Bowman's Capsule, Glomerulosclerosis, and Increased Fibrosis in *Trxrd2*^{iECKO} Mice. Further histopathological examination of hematoxylin/eosin (H&E)-stained tissue sections revealed a significant thickening of the Bowman's capsule in *Trxrd2*^{iECKO} mice compared to *Trxrd2*^{control} animals (Fig. 3*A*). Furthermore, a large number of glomeruli of *Trxrd2*^{iECKO} mice were completely (Fig. 3*B*, marked by a dashed line) or partially (*Inset* in Fig. 3*B*) sclerotized. Transmission electron microscopy also uncovered alterations of the glomerular basement membrane: e.g., hump-like structures as indicated in Fig. 3*C*. Furthermore, *Trxrd2*^{iECKO} mice showed an enhanced accumulation of collagen in the glomeruli-containing renal cortex, but not in the tubulointerstitial compartment of the kidney, as visualized by Sirius red staining (*SI Appendix*, Fig. S4).

EC Loss of *Trxrd2* Results in Renal Immune Cell Infiltrations. Analysis of PAS-stained kidney sections revealed infiltration of immune cells into the renal tissue of *Trxrd2*^{iECKO} mice (marked by a dashed line, Fig. 4 *A*, *Right*). Immunohistochemistry characterized these accumulated cells mainly as CD45-positive leukocytes (Fig. 4*B*). Immunohistochemistry using the macrophage marker MAC-2 with subsequent cell counting revealed significantly more MAC-2–positive cells within the tubulointerstitial as well as within the glomerular tissue of *Trxrd2*^{iECKO} mice compared to *Trxrd2*^{control} animals (Fig. 4*C*). No difference in the number of CD3-positive lymphocytes could be determined (WT: 123.2 ± 8.3 vs. KO: 109.8 ± 8.3 cells within 12 regions of interest [ROIs], $n = 5$ animals per group).

Analysis of Renal Function in *Trxrd2*^{iECKO} Mice. The observed histopathological findings in kidneys derived from *Trxrd2*^{iECKO} mice prompted us to analyze renal function by measuring the serum

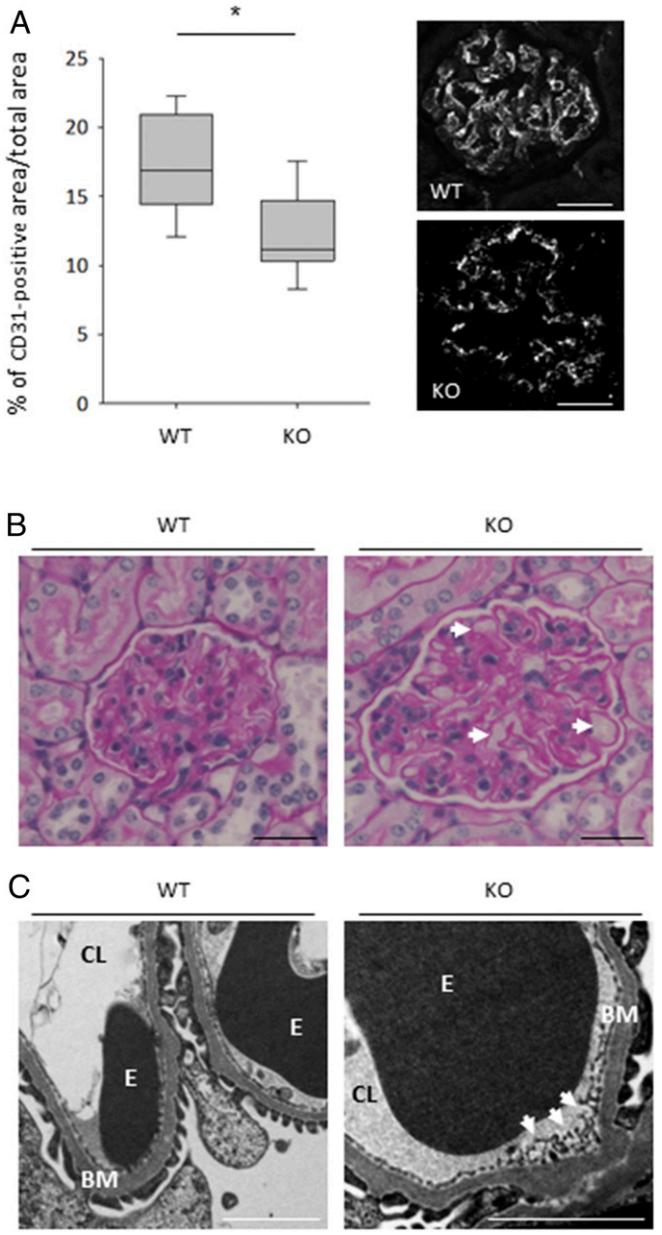

Fig. 2. Decreased glomerular capillary density and vascular alterations in *Trxrd2*^{iECKO} mice. (*A*) The capillary density of the glomeruli-containing area is significantly decreased in *Trxrd2*^{iECKO} mice. This is exemplified in the pictures on the *Right* by use of an antibody against CD31. $n = 7$ animals per group, *t* test. (Scale bar: 20 μm.) (*B*) PAS staining of the glomeruli reveals an enlargement of the capillary space in *Trxrd2*^{iECKO} mice (indicated by arrows). (Scale bar: 20 μm.) (*C*) Transmission electron microscopy confirms the vascular alterations by showing damage of the fenestrated ECs of the glomerular capillaries (white arrows). BM, basement membrane; CL, capillary lumen; E, erythrocyte. *$P < 0.05$. (Scale bar: 2,500 nm.)

creatinine and serum urea nitrogen concentrations. Both parameters were elevated in *Trxrd2*^{iECKO} mice (*SI Appendix*, Fig. S5). However, analysis of the urinary albumin-to-creatinine ratio (uACR) revealed no difference among the groups (*Trxrd2*^{control}: 31.2 ± 9.0 μg/mg vs. *Trxrd2*^{iECKO} mice: 46.9 ± 19.4 μg/mg, $n = 6$ animals per group, Mann–Whitney rank-sum test).

Peroxynitrite Levels Are Elevated in Vessels Derived from *Trxrd2*^{iECKO} Mice as Well as in *Trxrd2*$^{-/-}$ Cells. To gain further mechanistic insight into the role of TrxR2 in the endothelial compartment and to test whether the observed phenotype might be associated with elevated peroxynitrite levels, we analyzed freshly isolated mesenteric vessel segments (cut open to stain ECs) using the redox fluorescent probe fluorescein-boronate (Fl-B) that readily reacts with peroxynitrite (45, 46). Indeed, even under baseline conditions, vessels derived from *Trxrd2*^{iECKO} mice displayed a significantly higher fluorescence than those derived from *Trxrd2*^{control} mice (Fig. 5*A*). To assess whether the fluorescent signal was dependent on ·NO-derived peroxynitrite, cells were incubated with the endothelial nitric oxide synthase (eNOS) inhibitor *N*-nitro-L-arginine (LNA). Indeed, the fluorescence intensity decreased in *Trxrd2*^{iECKO} mice, but not in *Trxrd2*^{control} animals (Fig. 5*A*). On the contrary, incubation with LNA followed by the treatment with the ·NO-donor spermine NONOate (100 μM,

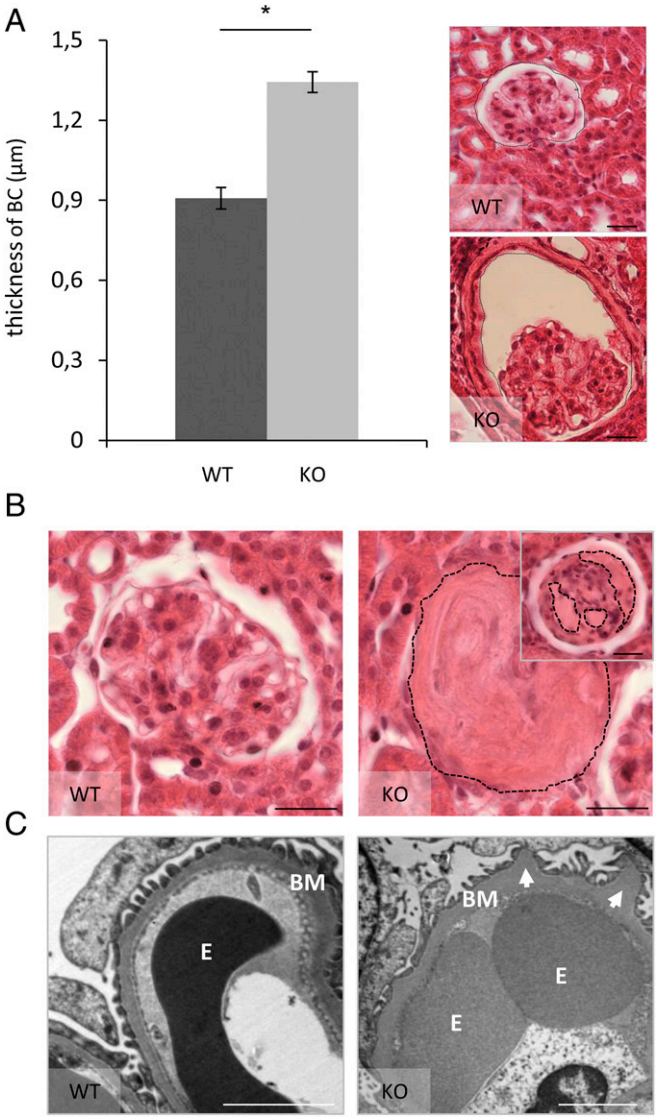

Fig. 3. Endothelial deletion of *Trxrd2* results in a number of renal pathologies. (*A*) *Trxrd2*^{iECKO} mice display significant thickening of the Bowman´s capsule (BC) compared to *Trxrd2*^{control} mice, as also exemplified by the pictures on the *Right*. $n = 5$ animals per group (*t* test). (Scale bar: 20 μm.) (*B*) *Trxrd2*^{iECKO} mice (*Right*) show a large number of completely (large figure) or partly (*Inset*) sclerotized glomeruli. Dashed lines mark sclerotized parts. (Scale bar: 20 μm.) (*C*) The glomerular basement membrane of *Trxrd2*^{iECKO} mice demonstrates in some cases hump-like swellings, as marked by arrows and visualized by transmission electron microscopy. E, erythrocyte; BM, basement membrane. *$P < 0.05$. (Scale bars: 2,500 nm.)

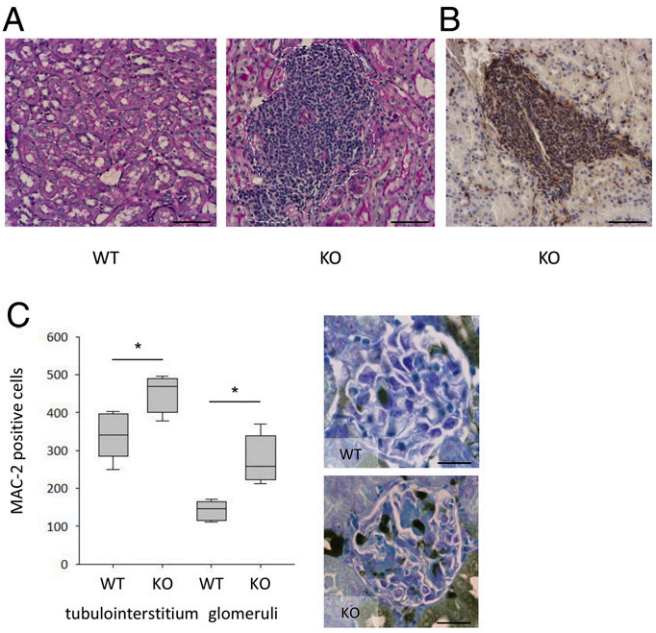

Fig. 4. Glomerular as well as tubulointerstitial immune cell infiltrations in *Trxrd2*^{iECKO} mice. (*A*) PAS-staining reveals infiltration of immune cells (marked by a dashed line) into the kidney of *Trxrd2*^{iECKO} mice. (Scale bar: 50 μm.) (*B*) Immunohistochemistry demonstrates that these infiltrated cells express the common leukocyte antigen CD45 (brown color). (Scale bar: 50 μm.) (*C*) Immunohistochemistry using the macrophage marker MAC-2 with subsequent cell counting shows a significantly enhanced number of macrophages within the tubulointerstitial as well as within the glomerular tissue of *Trxrd2*^{iECKO} mice, compared to control animals. The microphotographs on the *Right* show MAC-2–positive macrophages (brown color) within a glomerulus. $n = 5$ animals per group, *t* test. $^*P < 0.05$. (Scale bar: 20 μm.)

$t_{1/2}$ = 230 min at 25 °C and pH 7.4 ·NO flux ∼ 0.4 μM/min) (47) resulted in a significant increase of the fluorescent signal in *Trxrd2*^{control} mice compared to control conditions (Fig. 5*A*). In *Trxrd2*^{iECKO} mice, the combinatory incubation of LNA and NONOate elevated the signal again back to the level of control conditions (Fig. 5*A*). In addition, we analyzed the level of peroxynitrite in ECs isolated from the lung tissue of *Trxrd2*^{iECKO} and *Trxrd2*^{control} mice as well as in *Trxrd2*$^{+/+}$ and *Trxrd2*$^{-/-}$ embryonic endothelial progenitor cells (eEPCs) (13) using the Fl-B probe. Statistically significant higher steady-state levels of peroxynitrite were detected in ECs isolated from *Trxrd2*^{iECKO} mice compared to ECs isolated from *Trxrd2*^{control} mice (*SI Appendix*, Fig. S6*A*). In accordance, *Trxrd2*$^{-/-}$ eEPCs also displayed significantly higher levels of peroxynitrite than *Trxrd2*$^{+/+}$ cells (*SI Appendix*, Fig. S6*B*).

Enhanced Protein Tyrosine Nitration in Renal Tissue of *Trxrd2*^{iECKO} Mice. Since peroxynitrite is a powerful oxidant and nitrating agent with the capacity to oxidatively modify tyrosine (Tyr) to 3-nitrotyrosine (3-NO_2Tyr) (29), elevated peroxynitrite levels in vascular endothelium would consequently result in enhanced protein tyrosine nitration. Therefore, we examined renal tissue with an anti-nitrotyrosine antibody. Indeed, immunohistochemistry revealed a strong staining intensity in renal tissue derived from *Trxrd2*^{iECKO} mice. High immunopositive areas were evident, particularly in glomeruli as well as in renal parts with immune cell infiltrations (Fig. 5*B*). Immunoblotting using an antibody against nitrotyrosine confirmed enhanced protein nitration in renal tissue of *Trxrd2*^{iECKO} mice (Fig. 5*C*). Densitometric analysis of immunoblots revealed a 4.15 ± 0.8 times higher expression level in kidney tissue derived from *Trxrd2*^{iECKO} mice ($n = 6$ animals per group).

Expression Levels of Trx2, Grx2, Prx3, and Prx5 in *Trxrd2* Knockout Cells. The mitochondria-localized Prx3 was recently shown to rapidly reduce peroxynitrite (7). Interestingly, TrxR2 is necessary for maintaining Trx2 in its reduced state and, in turn, Prx3 uses both, Trx2 and Grx2 as electron donors (10). Therefore, we analyzed whether Trx2, Grx2, Prx3, and Prx5 expression levels were changed in *Trxrd2*$^{-/-}$ cells as compared to control cells. Immunoblotting under reducing conditions revealed that *Trxrd2*$^{-/-}$ eEPCs expressed higher levels of Grx2 (Fig. 6*A*) than *Trxrd2*$^{+/+}$ eEPCs (densitometric analysis revealed a 6.9 ± 2.3 higher expression level in *Trxrd2*$^{-/-}$ eEPCs, $n = 4$ immunoblots) whereas the levels of Trx2, Prx3, and Prx5 were not different between *Trxrd2* wild-type and knockout cells (Fig. 6*A*).

Deletion of *Trxrd2* Affects the Redox State of Prx3 and Enhances Prx3 Hyperoxidation. Since Grx2 can also reduce mitochondrial Prx3, we assessed whether the peroxiredoxin system is impaired in the *Trxrd2*$^{-/-}$ cells by analyzing the redox state of Prx3. Monitoring the ratio of Prx3 monomer and dimer revealed that, in *Trxrd2*$^{-/-}$ cells, Prx3 almost exclusively appears in its oxidized form (dimer) whereas *Trxrd2*$^{+/+}$ cells do contain both the reduced (monomer) as well as the oxidized (dimer) form (Fig. 6*B*). Analysis of Prx hyperoxidation by use of an antibody against peroxiredoxin-SO_3 (Prx-SO_3) showed an increased signal in *Trxrd2*$^{-/-}$ cells (Fig. 6*C*). However, the antibody against Prx-SO_3 cannot determine which of the peroxiredoxins is hyperoxidized. Therefore, we measured Prx3 hyperoxidation according to the method described by Cox et al. (48). This method takes advantage of the fact that, in the absence of alkylation, reduced Prxs immediately dimerize following cell lysis. However, hyperoxidized Prxs are unable to dimerize and remain as monomers. An immunoblot under nonreducing conditions shows that *Trxrd2*$^{-/-}$ cells display a higher level of monomers, hence more hyperoxidized Prx3 than *Trxrd*$^{+/+}$ cells (Fig. 6*D*). Thus, the near sevenfold compensatory increase of Grx2 was not sufficient to impede Prx3 oxidation and, in general, peroxiredoxin hyperoxidation. Analysis of the ratio of Grx2 monomer and dimer revealed that, in *Trxrd2*$^{-/-}$ cells, both forms, but especially the active monomer, show increased expression levels compared to control cells (Fig. 6*E*).

Kinetic Determination of the Reaction of Mitochondria Peroxy Yellow 1 with Peroxynitrite. Since TrxR2 is mainly located in the mitochondria, we explored whether the enhanced peroxynitrite levels might be preferentially generated in this organelle. Therefore, we initially characterized mitochondria peroxy yellow 1 (MitoPY1), a mitochondrial-targeted boronate-based compound initially reported as a hydrogen peroxide probe (49) [with a very small second order rate constant (∼0.2 $M^{-1}{\cdot}s^{-1}$) (49)], and evaluated if it could be used for mitochondrial-peroxynitrite detection. Indeed, as it has been well established that boronate-derived probes react very fast with peroxynitrite (45, 50, 51), we likewise determined the kinetics of the reaction of MitoPY1 with peroxynitrite. Indeed, direct kinetic analysis (Fig. 7 *A* and *B*) and competition kinetics (Table 1) showed that MitoPY1 readily reacts (k ∼10^6 $M^{-1}{\cdot}s^{-1}$) with peroxynitrite anion ($ONOO^-$).

The direct measurement (Fig. 7) provided a second order rate constant value of 0.7 × 10^6 $M^{-1}{\cdot}s^{-1}$ at 25 °C and pH 7.4. Alternatively, simple competition kinetic analysis for the oxidation of MitoPY1 by peroxynitrite in the presence of phenylalanine boronic acid (FBA) was performed and confirmed the rate constant value at 25 °C in the order of 10^6 $M^{-1}{\cdot}s^{-1}$ (Table 1).

We additionally tried to determine the rate constant of the reaction at 37 °C and pH of 7.8. Although the fittings were not as good as 25 °C, an estimated second order rate constant ∼0.8 × 10^6 $M^{-1}{\cdot}s^{-1}$ was obtained (Table 1). An important consideration is that it was found that the probe spontaneously emits fluorescence with time at 37 °C. Therefore, appropriate controls and careful data interpretation are essential.

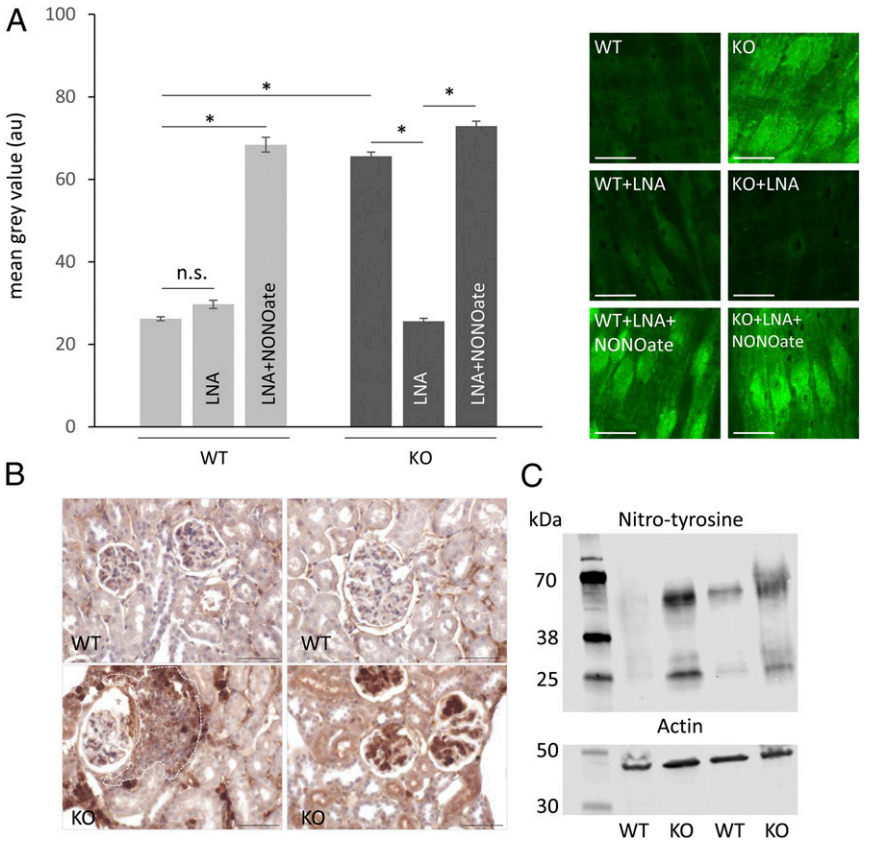

Fig. 5. Ex vivo detection of peroxynitrite in the endothelium and enhanced protein nitration in renal tissue of *Trxrd2*^{iECKO} mice. (*A*) Peroxynitrite detection by use of Fl-B probe reveals significantly higher peroxynitrite levels (indicated by a higher mean gray value [= higher fluorescence intensity]) in the vascular endothelium of vessels isolated from *Trxrd2*^{iECKO} mice compared to ECs of vessels isolated from *Trxrd2*^{control} mice (n = 8 animals per group). Treatment of isolated vessels from *Trxrd2*^{iECKO} mice with the eNOS inhibitor LNA (*N*-nitro-L-arginine) resulted in a significantly lowered fluorescence signal in *Trxrd2*^{iECKO}, but not in *Trxrd2*^{control} mice (n = 6 animals). The combinatory application of LNA and the ·NO-donor spermine NONOate significantly enhanced the fluorescence intensity in *Trxrd2*^{control} mice. In *Trxrd2*^{iECKO} mice, the combinatory incubation of LNA and NONOate elevated the signal to the level of control conditions (*A*) (n = 3 animals). ANOVA on ranks followed by all pairwise multiple comparison procedure. Pictures on the *Right* illustrate the observed fluorescence signal in the endothelium under the different conditions. au, arbitrary units. (Scale bar: 20 μm.) (*B*) Analysis of protein tyrosine nitration by use of an anti-nitrotyrosine antibody demonstrates basal staining in *Trxrd2*^{control} mice. *Trxrd2*^{iECKO} mice show an enhanced signal, especially in the glomeruli, but also in inflamed parts of the renal tissue derived from *Trxrd2*^{iECKO} mice, compared to renal tissue isolated from *Trxrd2*^{control} mice. (Scale bar: 50 μm.) (*C*) Immunoblotting using an antibody against nitrotyrosine demonstrates a stronger signal in renal tissue derived from *Trxrd2*^{iECKO} mice, indicating enhanced protein nitration in these animals. Actin served as a loading control. *P < 0.05. n.s., not significant.

Mitochondrial Localization of the Peroxynitrite Signal. Next, the mitochondrial-targeted probe MitoPY1 was tested on freshly isolated mesenteric vessel segments. Under baseline conditions, vessels derived from *Trxrd2*^{iECKO} mice displayed a significantly higher fluorescent intensity than those derived from *Trxrd2*^{control} mice (Fig. 7*C*). Adding LNA in order to block eNOS activity resulted in a significant decrease of the fluorescent signal in *Trxrd2*^{iECKO} mice (Fig. 7*C*). As a positive control, we added spermine NONOate to vessels derived from *Trxrd2*^{control} mice. This treatment resulted in a significant increase in the fluorescence intensity (Fig. 7*C*). The mitochondrial localization of the MitoPy1 signal was verified by use of a mitochondrial marker (*SI Appendix*, Fig. S7*A*).

The Peroxynitrite Decomposition Catalyst Mn(III)tetrakis(1-methyl-4-pyridyl) porphyrin Pentachloride Decreases Peroxynitrite Steady-State Levels. As a potential therapeutic strategy to decrease the peroxynitrite levels in ECs of *Trxrd2*^{iECKO} mice, we incubated freshly isolated mesenteric vessel segments with Mn(III)tetrakis(1-methyl-4-pyridyl)porphyrin pentachloride [Mn(III)TMPyP], a manganese-porphyrin which acts as a superoxide dismutase (SOD) mimetic (52) and mostly peroxynitrite decomposition catalyst (53–55). A protective role of manganese porphyrins against nitro-oxidative stress induced by the peroxynitrite donor 3-morpholinosydnonimine (SIN-1) has recently been demonstrated in ECs (56). Indeed, incubation with 25 μM Mn(III)TMPyP (55) for 2 h significantly decreased the fluorescent signal of the Fl-B probe in the vascular endothelium compared to saline-treated vessel segments (Fig. 8). Because the mean gray value in vessels derived from *Trxrd2*^{control} mice is low under baseline conditions, it is difficult to detect further lowering of the signal. Therefore, we used our cell culture system to test whether Mn(III) TMPyP has also an impact on control cells. Using the mitochondrial-targeted probe MitoPY1, we first verified its mitochondrial localization in eEPCs by use of a mitotracker (*SI Appendix*, Fig. S7*B*). Incubation with Mn(III)TMPyP (5μM) significantly lowered the fluorescence signal, both in wild-type as well as in *Trxrd2*$^{-/-}$ eEPCs (*SI Appendix*, Fig. S7*C*). Addition of NONOate significantly increased the signal in both cell types. When Mn(III)TMPyP was given in parallel, the signal could be significantly lowered but was not different from baseline levels (*SI Appendix*, Fig. S7*C*).

***Trxrd2*$^{-/-}$ Cells Are More Susceptible to Glutathione Depletion.** To test whether the enhanced Grx2 expression serves as a back-up system for the loss of *Trxrd2*, we examined the effects of experimental

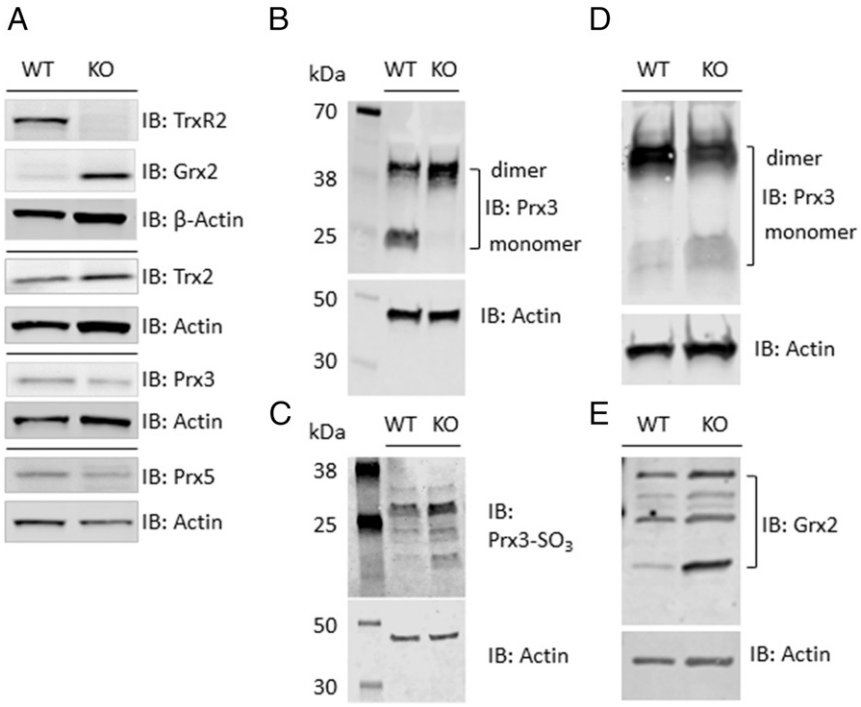

Fig. 6. Immunoblotting (IB) under reducing and nonreducing conditions. (*A*) Under reducing conditions immunoblotting demonstrates high levels of Grx2 in *Trxrd2*$^{-/-}$ eEPCs compared to wild-type cells. No difference was observed for the expression levels of Trx2, Prx3, and Prx5. (*B*) We monitored the redox state of Prx3 by alkylating the cells and analyzing them under nonreducing conditions. Whereas, in *Trxrd2*$^{-/-}$ cells, Prx3 almost exclusively appears in its oxidized form (dimer), *Trxrd2*$^{+/+}$ cells do contain both the reduced (monomer) as well as the oxidized form. (*C*) Analysis of Prx hyperoxidation by use of an antibody against Prx-SO_3 showed an increased signal in *Trxrd2*$^{-/-}$ cells. (*D*) In the absence of alkylation, we could demonstrate a higher level of monomers in *Trxrd2*$^{-/-}$ cells under nonreducing conditions, indicating that the amount of hyperoxidized Prx3 is higher in the *Trxrd2*$^{-/-}$ cells. (*E*) Analysis of the redox state of Grx2 revealed that *Trxrd2*$^{-/-}$ cells do have increased expression levels of both forms, the monomer as well as the dimer, but especially of the active monomer compared to control cells. Actin served as a loading control (*A*–*E*).

glutathione (GSH) depletion by applying buthionine sulphoximine (BSO) (400 nM), a highly specific and irreversible inhibitor of γ-glutamyl-cysteinyl-synthetase (γ-GCS), to the cell culture medium. Indeed, *Trxrd2*$^{-/-}$ eEPCs are much more susceptible to GSH depletion than wild-type cells as the number of viable cells [measured by use of a 3-(4,5-dimethylthiazol-2-yl)-2,5-diphenyltetrazolium bromide assay] was significantly lowered following 24 h treatment with BSO (*SI Appendix*, Fig. S8). The baseline level (no treatment) at 24 h was arbitrarily set to 100%. Addition of Mn(III)TMPyP (5 μM) to the BSO-treated cells increased the number of viable cells to the level of untreated cells. Treatment with Mn(III)TMPyP alone had no significant influence on cell viability (*SI Appendix*, Fig. S8). As an additional read-out for potential beneficial effects of Mn(III)TMPyP, we studied the mitochondrial membrane potential by using the dye JC-10. As shown previously (13), *Trxrd2*$^{-/-}$ cells have a significantly lower mitochondrial membrane potential than wild-type cells. We tested whether addition of Mn(III)TMPyP (5 μM, 24 h) could elevate the ratio of red-fluorescent JC-10 aggregates to monomeric, green fluorescent forms. However, addition of Mn(III)TMPyP alone had no impact on the JC-10 fluorescence ratio, neither in wild-type nor in *Trxrd2*$^{-/-}$ cells (*SI Appendix*, Fig. S9). Addition of BSO (400 nM, 24 h) significantly decreased the JC-10 ratio in knockout cells, but not in wild-type cells. Finally, a combination of both BSO and Mn(III)TMPyP was able to elevate the fluorescence ratio in *Trxrd2*$^{-/-}$ cells back to the control level (*SI Appendix*, Fig. S9). The mitochondrial oxidative phosphorylation uncoupler carbonyl cyanide-4-(trifluoromethoxy)phenylhydrazone served as a control substance and significantly lowered the JC-10 fluorescence ratio (WT: 0.37 ± 0.05; KO: 0.31 ± 0.05, $n = 6$ independent experiments).

Discussion

Endothelial cell dysfunction (ECD) was initially described as a defective endothelium-dependent vasorelaxation in patients at risk for the development of atherosclerosis (57–59). Today ECD sums up a broad number of vascular alterations: e.g., impaired antithrombogenic properties, increased expression of adhesion molecules and inflammatory genes, inappropriate regulation of vascular smooth muscle cell tone, or migratory properties (reviewed in refs. 60–63). However, the hallmark of ECD is still an impairment of ·NO-mediated endothelium-dependent vasodilation (23). TrxR2 deficiency in the endothelium results in impaired mitochondrial redox homeostasis and causes ECD (13). Interestingly, the observed vascular alterations are most pronounced in the kidney. Kidney eNOS is localized in the ECs of arteries and glomeruli and plays a series of functions, including regulation of vascular tone, sodium reabsorption, and renin release (64). Structural changes of the renal system (e.g., thickening of the glomerular basement membrane, glomerulosclerosis) are characteristics of an early stage of diabetic nephropathy (65–67), in which disruption of redox and ·NO metabolism and consequent nitroxidative stress have been observed (68–71). Moreover, some of the herein described glomerular alterations have also been detected in different forms of glomerulonephritis (72, 73).

In the present work, we aimed to analyze how the EC-specific deletion of *Trxrd2* affects vascular redox homeostasis and tissue integrity in different organs, thereby focusing on mitochondrial peroxynitrite formation and catabolism as a potential cause of the observed phenotype.

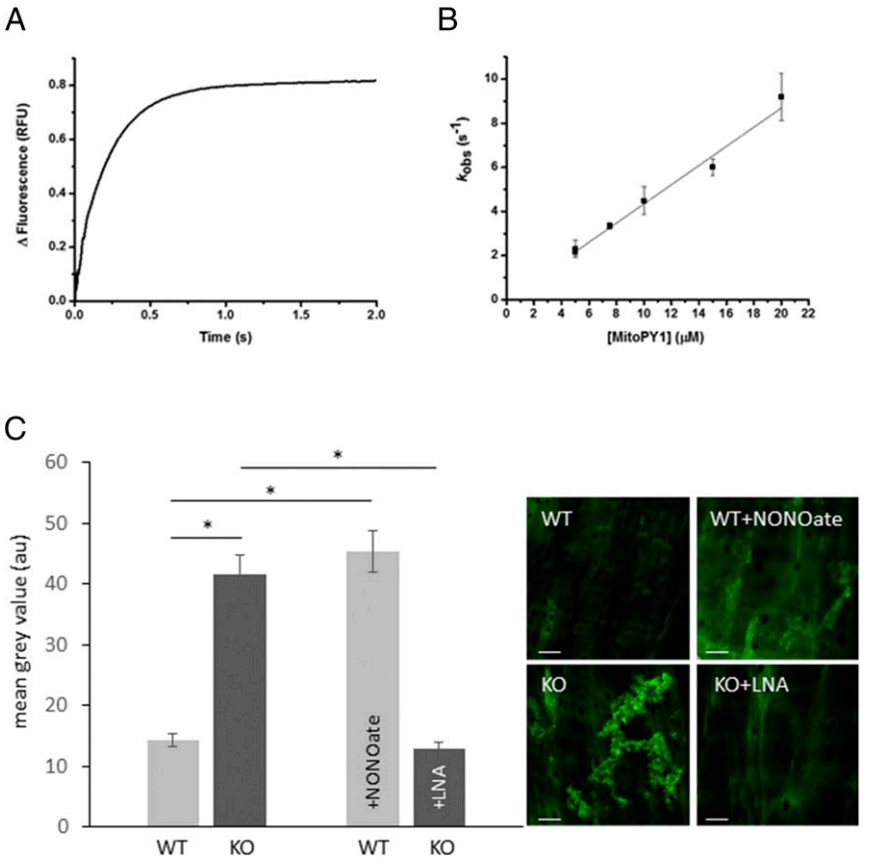

Fig. 7. MitoPY1 and mitochondrial peroxynitrite detection. (*A*) Time course of the fluorescence emission change upon oxidation of MitoPY1 (10 μM) by peroxynitrite (0.5 μM), as studied by stopped-flow techniques. RFU, relative fluorescence units. (*B*) Effect of increasing MitoPY1 concentrations on the observed rate constants (k_{obs}). All determinations were carried out in phosphate buffer (100 mM, pH 7.8, 0.1 mM diethylenetriaminepentaacetic acid) at 25 °C, and excitation was set at λ_{ex} = 503 nm and total emission recorded. (*C*) Use of MitoPY1 in ex vivo isolated vessels reveals significantly higher peroxynitrite levels in mitochondria of ECs derived from *Trxrd2*^{iECKO} mice compared to those isolated from *Trxrd2*^{control} mice ($n = 3$ animals per group). Treatment of vessels isolated from *Trxrd2*^{iECKO} mice with the eNOS inhibitor LNA significantly decreased the peroxynitrite detection in the mitochondria of ECs. On the opposite, addition of the ·NO-donor spermine NONOate significantly increased the peroxynitrite levels in the mitochondria of ECs isolated from *Trxrd2*^{control} mice. $n = 3$ animals per group. au, arbitrary units. ANOVA on ranks followed by all pairwise multiple comparison procedures. Pictures on the *Right* illustrate the observed fluorescence signal in the endothelium under the different conditions. *$P < 0.05$. (Scale bar: 10 μm.)

By using a highly sensitive redox probe, Fl-B (45, 74), we measured peroxynitrite ex vivo in the endothelial layer of isolated mesenteric arteries, showing significantly enhanced peroxynitrite levels compared to the endothelium of *Trxrd2*^{control} mice (Fig. 5*A*). While boronate-based fluorescent probes have been previously successfully used in cells (45, 46, 51) and model organisms, such as *Caenorhabditis elegans* (75) and zebrafish (76), herein, we report its application for redox imaging in mammalian tissues.

Although physiological levels of ·NO are essential for many aspects of vascular homeostasis (18–21), its interactions with vessel-derived $O_2^{\cdot-}$ can exert cytotoxic, proinflammatory and tissue disruptive effects by its oxidation product peroxynitrite (27–29). We hypothesized that, secondary to the perturbation of mitochondrial redox control due to the lack of TrxR2 activity, mitochondrial $O_2^{\cdot-}$ fluxes increase and most of the eNOS-derived ·NO is consumed to yield peroxynitrite, a process that parallels a decrease in ·NO bioavailability. This is supported by a less efficient response of arterioles in *Trxrd2*^{iECKO} mice to the vasodilators Ach and SNP. Such an impaired response was also described for heart vessels when perfused with peroxynitrite (77). In addition, oxidative stress can decrease the expression and activity of soluble guanylyl cyclase (sGC) in vascular smooth muscle cells (78). Peroxynitrite may act in a paracrine manner on surrounding vascular smooth muscle cells. This in turn could account for a diminished vascular response toward SNP in *Trxrd2*^{iECKO} mice.

Table 1. Rate constants for the reaction of peroxynitrite with MitoPY1 determined at 25 °C or 37 °C and pH 7.4 or pH 7.8, determined by direct measurement or competition approach

	Conditions, k ($M^{-1}\cdot s^{-1}$)		
Methodology	25 °C and pH 7.4	25 °C and pH 7.8	37 °C and pH 7.8
Direct	$(0.70 \pm 0.04) \times 10^6$	$(0.43 \pm 0.01) \times 10^6$	$(0.80 \pm 0.10) \times 10^6$
Competition	$(1.0 \pm 0.3) \times 10^6$	ND	ND

ND, not determined.

The observation of arterial hypertrophy and enhanced vascular stiffness in *Trxrd2*^{iECKO} mice (Fig. 1) is similar to changes in the arterial wall that have been observed, either following genetic deletion of eNOS in mice (79, 80) or following chronic inhibition of ·NO synthesis (81). Moreover, the impaired flow-dependent vasodilation in *Trxrd2*^{iECKO} mice (13) likely depends on an elevated ·NO consumption. Interestingly, whereas addition of eNOS inhibitors did not further decrease this impaired vasodilatory response of vessels derived from *Trxrd2*^{iECKO} mice supporting that most if not all of the ·NO was already being compromised (13), such ex vivo inhibition of ·NO production consequently led to significantly decreased peroxynitrite levels in the EC layer of vessels derived from *Trxrd2*^{iECKO} mice (Fig. 5*A*).

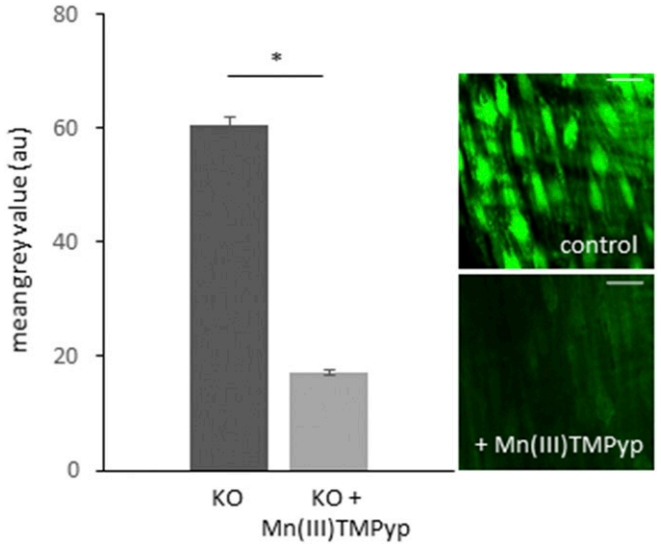

Fig. 8. Mn(III)TMPyP, a peroxynitrite decomposition catalyst, decreases peroxynitrite levels in vessels lacking endothelial TrxR2. Treatment of mesenteric vessel segments isolated from *Trxrd2*^{iECKO} mice with 25 μM Mn(III)TMPyP for 2 h significantly decreases peroxynitrite levels in the vascular endothelium, as detected by Fl-B. au, arbitrary units; $n = 3$ animals per group; Mann–Whitney rank-sum test. $^*P < 0.05$. (Scale bar: 20 μm.)

Peroxynitrite-derived radicals can lead to the nitration of protein tyrosine residues to 3-nitrotyrosine (27, 29, 82). An enhanced protein nitration in renal tissue of *Trxrd2*^{iECKO} mice further substantiated that ex vivo measured elevated steady-state levels of peroxynitrite correlated with their generation in vivo (Fig. 5*B*). One of the known targets for nitrating species in the vasculature (83) is prostacyclin synthase, which becomes inactivated by a site-specific nitration at Tyr-430 (29, 84). In this sense, peroxynitrite has the ability to block vasodilatory pathways mediated by prostacyclin.

In addition, several other candidate tyrosine nitrated proteins could account for part of the phenotypic changes encountered in the kidney including MnSOD (85, 86), p190RhoGAP-A (87), PKG (88), and eNOS itself (89) and should be explored in future proteomics-based analysis (90).

TrxR2 itself exists in three isoforms which differ in their N termini (91), with the predominant form containing an N-terminal signal peptide necessary for mitochondrial targeting (92–94), supporting the idea that defective mitochondrial peroxide catabolism by TrxR2 secondarily compromises mitochondrial function. Therefore, we analyzed whether mitochondrial levels of peroxynitrite were enhanced under conditions of TrxR2 deficiency. For this purpose, we used MitoPY1, a mitochondrial-targeted boronate-based compound initially reported as an H_2O_2 probe (49). Since boronate-derived probes react fast with peroxynitrite (45, 50, 51), we performed direct kinetic analysis, as well as competition kinetics, to prove that MitoPY1 readily reacts with the peroxynitrite anion (Fig. 7 *A* and *B* and Table 1). Subsequent ex vivo analysis verified that mitochondria of Txnrd2-deficient ECs were an important source of peroxynitrite (Fig. 7*C*). As the fluorescence arising from the boronate-based probe could be modulated by the use of NOS inhibitors and by the addition of ·NO donors, respectively, these experiments largely support that these responses were mediated by peroxynitrite (Fig. 7*C*).[‡] Hence, this is a demonstration linking peroxynitrite catabolism with TrxR2-dependent pathways in vivo.

A significant elevation of the steady-state levels of peroxynitrite is the result of two aberrant processes, which ultimately trigger a vicious cycle. First, the lack of TrxR2 compromises H_2O_2 detoxification through the Prx3/Trx2/TrxR2 axis (95, 96), and elevated H_2O_2 levels increase the calcium concentration in ECs, thereby stimulating excessive ·NO production through eNOS (97) and mitochondria-derived $O_2^{\cdot-}$ (98, 99). This initial event triggers mitochondrial peroxynitrite formation via the diffusion-controlled reaction of ·NO with $O_2^{\cdot-}$. Second, once peroxynitrite is generated, the lack of TrxR2 results in a failure of peroxynitrite elimination by either Prx3 or Prx5 (4, 5, 7), overall causing an elevation of steady-state levels and subsequent oxidation and nitration reactions, which further alter mitochondrial redox homeostasis (28) and EC function. For instance, peroxynitrite disrupts mitochondrial redox homeostasis and bioenergetics by mechanisms that include aconitase inactivation, inhibition of complex I and II-dependent electron transport, and MnSOD inactivation (28). Future work using mitochondrial probes for ·NO (100) and superoxide radicals (101) and the analysis of MnSOD nitration and inactivation will help to further assess the dynamics of the peroxynitrite formation in these model systems.

Since the observed phenotype is moderate, and not life threatening for the mice, it is possible that other systems partly compensate for the endothelial loss of TrxR2. Indeed, the mitochondrial-located Prx3 is not only a substrate for Trx2, but can also be reduced by Grx2, which is unique because it can receive electrons from both TrxR2 and GSH (102). Interestingly, our analysis revealed that *Trxrd2*$^{-/-}$ cells express significantly higher levels of Grx2 (Fig. 6*A*). Even though immunoblots under nonreducing conditions confirmed high levels of the active Grx2 monomer in *Trxrd2*$^{-/-}$ cells (Fig. 6*E*), analysis of the redox state of Prx3 showed a strong accumulation of the oxidized protein. In contrast, *Trxrd2*$^{+/+}$ cells do contain both, the reduced as well as the oxidized form (Fig. 6*B*). This is striking because silencing the expression of either Trx2 or Grx2 in HeLa cells using specific small interfering RNA (siRNA) did not change the monomer:-dimer ratio of Prx3 (10). In parallel, we observed an enhanced accumulation of hyperoxidized Prx3, further indicating sustained oxidative conditions in *Trxrd2*$^{-/-}$ cells (Fig. 6*D*). The second mitochondria-located peroxiredoxin, Prx5, is a member of the atypical 2-Cys Prxs (103) and fully relies on the Trx system for the reduction of the disulfide formed during its reaction cycle (10). Its expression level was not altered in the knockout context (Fig. 6*A*). To analyze whether Prx3 partially copes with mitochondrial peroxides via the glutaredoxin-dependent redox pathway[§] in TrxR2-deficient cells, we deprived cells of GSH using BSO, a highly specific and irreversible inhibitor of γ-GCS. The observed significant decrease of cell viability (*SI Appendix*, Fig. S8) supported our hypothesis.

As a final proof that vascular peroxynitrite was enhanced in TrxR2-deficient ECs, we pretreated vessels with a cell-permeable Mn-porphyrin to pharmacologically eliminate peroxynitrite. Indeed, Mn-porphyrins including Mn(III)TMPyP are known to catalytically reduce peroxynitrite to nitrite at the expense of reducing equivalents arising from various sources, including the mitochondrial electron transport chain and low molecular weight compounds (28, 104, 105). In particular, cationic Mn-porphyrins can permeate mitochondria (55) in the oxidized state (Mn^{3+}) which, upon reduction in mitochondria (Mn^{2+}), is the actual reactant with peroxynitrite; Mn-porphyrins can easily reach micromolar levels in mitochondria and exert strong cytoprotective actions against peroxynitrite (56). In our work, Mn(III)TMPyP significantly decreased peroxynitrite detection in the *Trxrd2*^{iECKO} vessels

[‡]The residual fluorescence in the presence of the NOS inhibitors may be attributed to mitochondrial H_2O_2.

[§]Glutaredoxin reduction depends, in turn, on glutathione and glutathione reductase.

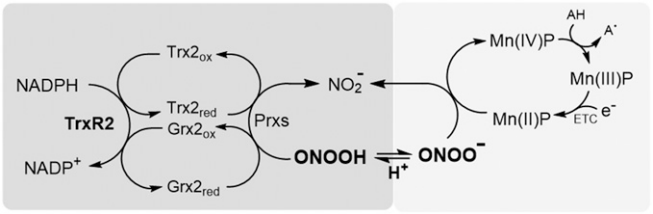

Fig. 9. TrxR2-mediated detoxification of peroxynitrite in mitochondria and manganese porphyrin-based pharmacology. The left-hand part of the scheme shows how TrxR2 fuels electrons from NADPH to Trx2, which, in turn, reduces mitochondrial Prx3 and Prx5 (Prxs). Interestingly, TrxR2 can also reduce the mitochondrial glutaredoxin (Grx2) that can also serve as the proximal electron donor to Prx3 (10). The mitochondrial peroxiredoxins readily reduce peroxynitrous acid to nitrite via their fast reacting peroxidatic thiols, with second order rate constants of 1×10^7 and 1.2×10^8 $M^{-1} \cdot s^{-1}$, respectively (4). The right-hand part of the scheme shows that MnP in the 2+ redox state catalytically reduces the peroxynitrite anion to nitrite at the expense of reducing equivalents of endogenous reductants, such as glutathione and the electron transport chain (104, 105). The pK_a of peroxynitrite is 6.8; thus, both peroxynitrous acid and the peroxynitrite anion are present and in rapid acid–base equilibrium in mitochondria. AH, reductant; ETC, electron transport chain; ox, oxidized; red, reduced.

(Fig. 8), but also in *Trxrd2*$^{-/-}$ and control cells (*SI Appendix*, Fig. S7), in full agreement with its role as a peroxynitrite decomposition catalyst. It is likely that long-term Mn-porphyrin therapy may serve to attenuate the vascular phenotype in the *Trxrd2*^{iECKO} animals.

Conclusions

In sum, our work shows that endothelial TrxR2 controls vascular integrity and that its targeted loss is associated with a disruption of both ·NO and redox homeostasis, leading to elevated steady-state levels of peroxynitrite. The enhanced formation of peroxynitrite reflects the compromised bioavailability of ·NO by its $O_2^{\cdot-}$ mediated oxidative inactivation under conditions of TrxR2 deficiency (106) and, at the same time, represents a feasible pathogenic mechanism accounting for the loss of tissue integrity. Thus, TrxR2 represents a central control point of intramitochondrial and intracellular peroxynitrite levels, and Mn-porphyrins pharmacologically assist to detoxify mitochondrial peroxynitrite under conditions of vascular nitroxidative stress (Fig. 9).

Materials and Methods

Generation of *Trxrd2*^{iECKO} Mice. To analyze the biological significance of TrxR2 expression and activity in vascular ECs in vivo, we interbred *Trxrd2*$^{lox/lox}$ mice (11) with transgenic mice expressing the tamoxifen-inducible recombinase CreERT2 under control of the endothelial Cdh5 promoter (a kind gift from Ralf Adams, Max Planck Institute for Molecular Biomedicine, Münster, Germany) (107). These mice were further crossed with *Trxrd2*$^{lox/lox}$, *Trxrd2*$^{lox/wt}$, and *Trxrd2*$^{wt/wt}$ mice to generate litters containing *Trxrd2*$^{lox/lox}$*Cdh5(PAC)-CreERT2* (referred to as *Trxrd2*^{iECKO} [KO]) and control littermates (referred to as *Trxrd2*^{control} [WT]). All animal experiments were approved by the local animal ethics committees (Regierung von Oberbayern, Munich, Germany; Ministerium für Energiewende, Landwirtschaft, Umwelt, Natur und Digitalisierung, Kiel, Germany).

Statistical Analysis. Statistical analysis was performed using SigmaPlot 13.0 software (Jandel GmbH, Erkrath, Germany). In the bar diagrams, experimental values are expressed as mean ± SEM unless otherwise stated (all box and whisker plots show the median). The statistical tests, as well as the number of independent experiments, are indicated in the corresponding part of the results section or in the figure legend. A nonparametric test was applied when data did not pass a normality test. A $P < 0.05$ was considered significant and denoted in the figures by an asterisk (*).

Further materials and methods can be found in *SI Appendix*.

Data Availability. All study data are included in the article and/or *SI Appendix*.

ACKNOWLEDGMENTS. We thank Dorothee Gössel, Ursula Keller, Dora Kiesl, and Matthias Semisch for excellent technical assistance. This work was supported by the Deutsche Forschungsgemeinschaft Priority Programme SPP 1190 (to H.B. and M.C.), the Friedrich-Baur Stiftung (to H.B.), and grants from Universidad de la República (Espacio Interdisciplinario 2015 and CSIC_Grupos 2018) (to R.R.). Additional support was obtained from Programa de Desarrollo de Ciencias Basicas. N.R. and A.M.R. were supported partially by fellowships from Agencia Nacional de Investigación e Innovación and Universidad de la República, Uruguay.

1. J. Lu, A. Holmgren, The thioredoxin antioxidant system. *Free Radic. Biol. Med.* **66**, 75–87 (2014).
2. E. S. Arner, A. Holmgren, Physiological functions of thioredoxin and thioredoxin reductase. *Eur. J. Biochem.* **267**, 6102–6109 (2000).
3. H. Zhang *et al.*, Endothelial-specific expression of mitochondrial thioredoxin improves endothelial cell function and reduces atherosclerotic lesions. *Am. J. Pathol.* **170**, 1108–1120 (2007).
4. A. Zeida *et al.*, Catalysis of peroxide reduction by fast reacting protein thiols. *Chem. Rev.* **119**, 10829–10855 (2019).
5. M. Dubuisson *et al.*, Human peroxiredoxin 5 is a peroxynitrite reductase. *FEBS Lett.* **571**, 161–165 (2004).
6. M. Trujillo *et al.*, Pre-steady state kinetic characterization of human peroxiredoxin 5: Taking advantage of Trp84 fluorescence increase upon oxidation. *Arch. Biochem. Biophys.* **467**, 95–106 (2007).
7. M. I. De Armas *et al.*, Rapid peroxynitrite reduction by human peroxiredoxin 3: Implications for the fate of oxidants in mitochondria. *Free Radic. Biol. Med.* **130**, 369–378 (2019).
8. S. Watabe *et al.*, SP-22 is a thioredoxin-dependent peroxide reductase in mitochondria. *Eur. J. Biochem.* **249**, 52–60 (1997).
9. B. Knoops, J. Goemaere, V. Van der Eecken, J. P. Declercq, Peroxiredoxin 5: Structure, mechanism, and function of the mammalian atypical 2-Cys peroxiredoxin. *Antioxid. Redox Signal.* **15**, 817–829 (2011).
10. E. M. Hanschmann *et al.*, Both thioredoxin 2 and glutaredoxin 2 contribute to the reduction of the mitochondrial 2-Cys peroxiredoxin Prx3. *J. Biol. Chem.* **285**, 40699–40705 (2010).
11. M. Conrad *et al.*, Essential role for mitochondrial thioredoxin reductase in hematopoiesis, heart development, and heart function. *Mol. Cell. Biol.* **24**, 9414–9423 (2004).
12. J. Horstkotte *et al.*, Mitochondrial thioredoxin reductase is essential for early postischemic myocardial protection. *Circulation* **124**, 2892–2902 (2011).
13. J. Kirsch *et al.*, Endothelial dysfunction, and A prothrombotic, proinflammatory phenotype is caused by loss of mitochondrial thioredoxin reductase in endothelium. *Arterioscler. Thromb. Vasc. Biol.* **36**, 1891–1899 (2016).
14. N. Panth, K. R. Paudel, K. Parajuli, Reactive oxygen species: A key hallmark of cardiovascular disease. *Adv. Med.* **2016**, 9152732 (2016).
15. J. E. Deanfield, J. P. Halcox, T. J. Rabelink, Endothelial function and dysfunction: Testing and clinical relevance. *Circulation* **115**, 1285–1295 (2007).
16. D. Tousoulis, A. M. Kampoli, C. Tentolouris, N. Papageorgiou, C. Stefanadis, The role of nitric oxide on endothelial function. *Curr. Vasc. Pharmacol.* **10**, 4–18 (2012).
17. S. Moncada, Nitric oxide in the vasculature: Physiology and pathophysiology. *Ann. N. Y. Acad. Sci.* **811**, 60–67, discussion 67–69 (1997).
18. P. M. Bath, D. G. Hassall, A. M. Gladwin, R. M. Palmer, J. F. Martin, Nitric oxide and prostacyclin. Divergence of inhibitory effects on monocyte chemotaxis and adhesion to endothelium in vitro. *Arterioscler. Thromb.* **11**, 254–260 (1991).
19. R. De Caterina *et al.*, Nitric oxide decreases cytokine-induced endothelial activation. Nitric oxide selectively reduces endothelial expression of adhesion molecules and proinflammatory cytokines. *J. Clin. Invest.* **96**, 60–68 (1995).
20. R. Bhardwaj, C. P. Page, G. R. May, P. K. Moore, Endothelium-derived relaxing factor inhibits platelet aggregation in human whole blood in vitro and in the rat in vivo. *Eur. J. Pharmacol.* **157**, 83–91 (1988).
21. J. Lei, Y. Vodovotz, E. Tzeng, T. R. Billiar, Nitric oxide, a protective molecule in the cardiovascular system. *Nitric Oxide* **35**, 175–185 (2013).
22. D. G. Harrison, Cellular and molecular mechanisms of endothelial cell dysfunction. *J. Clin. Invest.* **100**, 2153–2157 (1997).
23. J. Davignon, P. Ganz, Role of endothelial dysfunction in atherosclerosis. *Circulation* **109**, III27–III32 (2004).
24. P. L. Huang *et al.*, Hypertension in mice lacking the gene for endothelial nitric oxide synthase. *Nature* **377**, 239–242 (1995).
25. R. J. Gryglewski, R. M. Palmer, S. Moncada, Superoxide anion is involved in the breakdown of endothelium-derived vascular relaxing factor. *Nature* **320**, 454–456 (1986).
26. L. J. Ignarro, G. M. Buga, K. S. Wood, R. E. Byrns, G. Chaudhuri, Endothelium-derived relaxing factor produced and released from artery and vein is nitric oxide. *Proc. Natl. Acad. Sci. U.S.A.* **84**, 9265–9269 (1987).
27. P. Pacher, J. S. Beckman, L. Liaudet, Nitric oxide and peroxynitrite in health and disease. *Physiol. Rev.* **87**, 315–424 (2007).
28. R. Radi, Oxygen radicals, nitric oxide, and peroxynitrite: Redox pathways in molecular medicine. *Proc. Natl. Acad. Sci. U.S.A.* **115**, 5839–5848 (2018).
29. G. Ferrer-Sueta *et al.*, Biochemistry of peroxynitrite and protein tyrosine nitration. *Chem. Rev.* **118**, 1338–1408 (2018).

30. M. H. Zou, C. Shi, R. A. Cohen, Oxidation of the zinc-thiolate complex and uncoupling of endothelial nitric oxide synthase by peroxynitrite. *J. Clin. Invest.* **109**, 817–826 (2002).
31. J. B. Laursen *et al*., Endothelial regulation of vasomotion in apoE-deficient mice: Implications for interactions between peroxynitrite and tetrahydrobiopterin. *Circulation* **103**, 1282–1288 (2001).
32. C. Quijano, L. Castro, G. Peluffo, V. Valez, R. Radi, Enhanced mitochondrial superoxide in hyperglycemic endothelial cells: Direct measurements and formation of hydrogen peroxide and peroxynitrite. *Am. J. Physiol. Heart Circ. Physiol.* **293**, H3404–H3414 (2007).
33. U. Förstermann, Oxidative stress in vascular disease: Causes, defense mechanisms and potential therapies. *Nat. Clin. Pract. Cardiovasc. Med.* **5**, 338–349 (2008).
34. C. F. Mueller, K. Laude, J. S. McNally, D. G. Harrison, ATVB in focus: Redox mechanisms in blood vessels. *Arterioscler. Thromb. Vasc. Biol.* **25**, 274–278 (2005).
35. M. Conrad, Transgenic mouse models for the vital selenoenzymes cytosolic thioredoxin reductase, mitochondrial thioredoxin reductase and glutathione peroxidase 4. *Biochim. Biophys. Acta* **1790**, 1575–1585 (2009).
36. Y. Li *et al*., Dilated cardiomyopathy and neonatal lethality in mutant mice lacking manganese superoxide dismutase. *Nat. Genet.* **11**, 376–381 (1995).
37. L. Nonn, R. R. Williams, R. P. Erickson, G. Powis, The absence of mitochondrial thioredoxin 2 causes massive apoptosis, exencephaly, and early embryonic lethality in homozygous mice. *Mol. Cell. Biol.* **23**, 916–922 (2003).
38. M. Matsui *et al*., Early embryonic lethality caused by targeted disruption of the mouse thioredoxin gene. *Dev. Biol.* **178**, 179–185 (1996).
39. W. Zhang *et al*., Endothelial cell-specific liver kinase B1 deletion causes endothelial dysfunction and hypertension in mice in vivo. *Circulation* **129**, 1428–1439 (2014).
40. M. Wortmann *et al*., Combined deficiency in glutathione peroxidase 4 and vitamin E causes multiorgan thrombus formation and early death in mice. *Circ. Res.* **113**, 408–417 (2013).
41. L. V. d'Uscio *et al*., Mechanisms of vascular dysfunction in mice with endothelium-specific deletion of the PPAR-δ gene. *Am. J. Physiol. Heart Circ. Physiol.* **306**, H1001–H1010 (2014).
42. C. Espinosa-Díez *et al*., Role of glutathione biosynthesis in endothelial dysfunction and fibrosis. *Redox Biol.* **14**, 88–99 (2018).
43. P. Patwari, R. T. Lee, Thioredoxins, mitochondria, and hypertension. *Am. J. Pathol.* **170**, 805–808 (2007).
44. B. M. Kaess *et al*., Aortic stiffness, blood pressure progression, and incident hypertension. *JAMA* **308**, 875–881 (2012).
45. N. Rios *et al*., Sensitive detection and estimation of cell-derived peroxynitrite fluxes using fluorescein-boronate. *Free Radic. Biol. Med.* **101**, 284–295 (2016).
46. C. Prolo, N. Rios, L. Piacenza, M. N. Álvarez, R. Radi, Fluorescence and chemiluminescence approaches for peroxynitrite detection. *Free Radic. Biol. Med.* **128**, 59–68 (2018).
47. M. N. Alvarez, M. Trujillo, R. Radi, Peroxynitrite formation from biochemical and cellular fluxes of nitric oxide and superoxide. *Methods Enzymol.* **359**, 353–366 (2002).
48. A. G. Cox, C. C. Winterbourn, M. B. Hampton, Measuring the redox state of cellular peroxiredoxins by immunoblotting. *Methods Enzymol.* **474**, 51–66 (2010).
49. B. C. Dickinson, C. J. Chang, A targetable fluorescent probe for imaging hydrogen peroxide in the mitochondria of living cells. *J. Am. Chem. Soc.* **130**, 9638–9639 (2008).
50. A. Sikora, J. Zielonka, M. Lopez, J. Joseph, B. Kalyanaraman, Direct oxidation of boronates by peroxynitrite: Mechanism and implications in fluorescence imaging of peroxynitrite. *Free Radic. Biol. Med.* **47**, 1401–1407 (2009).
51. J. Zielonka, A. Sikora, J. Joseph, B. Kalyanaraman, Peroxynitrite is the major species formed from different flux ratios of co-generated nitric oxide and superoxide: Direct reaction with boronate-based fluorescent probe. *J. Biol. Chem.* **285**, 14210–14216 (2010).
52. K. M. Faulkner, S. I. Liochev, I. Fridovich, Stable Mn(III) porphyrins mimic superoxide dismutase in vitro and substitute for it in vivo. *J. Biol. Chem.* **269**, 23471–23476 (1994).
53. G. Ferrer-Sueta *et al*., Reactions of manganese porphyrins with peroxynitrite and carbonate radical anion. *J. Biol. Chem.* **278**, 27432–27438 (2003).
54. G. Ferrer-Sueta, C. Quijano, B. Alvarez, R. Radi, Reactions of manganese porphyrins and manganese-superoxide dismutase with peroxynitrite. *Methods Enzymol.* **349**, 23–37 (2002).
55. I. Batinić-Haberle *et al*., Pure MnTBAP selectively scavenges peroxynitrite over superoxide: Comparison of pure and commercial MnTBAP samples to MnTE-2-PyP in two models of oxidative stress injury, an SOD-specific Escherichia coli model and carrageenan-induced pleurisy. *Free Radic. Biol. Med.* **46**, 192–201 (2009).
56. S. Carballal *et al*., Manganese porphyrin redox state in endothelial cells: Resonance Raman studies and implications for antioxidant protection towards peroxynitrite. *Free Radic. Biol. Med.* **126**, 379–392 (2018).
57. A. M. Zeiher, H. Drexler, H. Wollschläger, H. Just, Modulation of coronary vasomotor tone in humans. Progressive endothelial dysfunction with different early stages of coronary atherosclerosis. *Circulation* **83**, 391–401 (1991).
58. K. G. Reddy, R. N. Nair, H. M. Sheehan, J. M. Hodgson, Evidence that selective endothelial dysfunction may occur in the absence of angiographic or ultrasound atherosclerosis in patients with risk factors for atherosclerosis. *J. Am. Coll. Cardiol.* **23**, 833–843 (1994).
59. A. A. Quyyumi *et al*., Nitric oxide activity in the human coronary circulation. Impact of risk factors for coronary atherosclerosis. *J. Clin. Invest.* **95**, 1747–1755 (1995).
60. C. Rask-Madsen, G. L. King, Mechanisms of disease: Endothelial dysfunction in insulin resistance and diabetes. *Nat. Clin. Pract. Endocrinol. Metab.* **3**, 46–56 (2007).
61. C. M. Sena, A. M. Pereira, R. Seiça, Endothelial dysfunction–A major mediator of diabetic vascular disease. *Biochim. Biophys. Acta* **1832**, 2216–2231 (2013).
62. M. A. Gimbrone, Jr, G. García-Cardeña, Endothelial cell dysfunction and the pathobiology of atherosclerosis. *Circ. Res.* **118**, 620–636 (2016).
63. S. Taddei, L. Ghiadoni, A. Virdis, D. Versari, A. Salvetti, Mechanisms of endothelial dysfunction: Clinical significance and preventive non-pharmacological therapeutic strategies. *Curr. Pharm. Des.* **9**, 2385–2402 (2003).
64. S. Lamas, D. Rodríguez-Puyol, Endothelial control of vasomotor tone: The kidney perspective. *Semin. Nephrol.* **32**, 156–166 (2012).
65. R. Osterby, H. J. Gundersen, Glomerular size and structure in diabetes mellitus. I. Early abnormalities. *Diabetologia* **11**, 225–229 (1975).
66. F. Mac-Moune Lai *et al*., Isolate diffuse thickening of glomerular capillary basement membrane: A renal lesion in prediabetes? *Mod. Pathol.* **17**, 1506–1512 (2004).
67. A. M. Cusumano *et al*., Glomerular hypertrophy is associated with hyperinsulinemia and precedes overt diabetes in aging rhesus monkeys. *Am. J. Kidney Dis.* **40**, 1075–1085 (2002).
68. G. Peluffo, R. Radi, Biochemistry of protein tyrosine nitration in cardiovascular pathology. *Cardiovasc. Res.* **75**, 291–302 (2007).
69. A. S. De Vriese, T. J. Verbeuren, J. Van de Voorde, N. H. Lameire, P. M. Vanhoutte, Endothelial dysfunction in diabetes. *Br. J. Pharmacol.* **130**, 963–974 (2000).
70. C. Szabo, Role of nitrosative stress in the pathogenesis of diabetic vascular dysfunction. *Br. J. Pharmacol.* **156**, 713–727 (2009).
71. P. Pacher, I. G. Obrosova, J. G. Mabley, C. Szabó, Role of nitrosative stress and peroxynitrite in the pathogenesis of diabetic complications. Emerging new therapeutical strategies. *Curr. Med. Chem.* **12**, 267–275 (2005).
72. S. Sethi, F. C. Fervenza, Standardized classification and reporting of glomerulonephritis. *Nephrol. Dial. Transplant.* **34**, 193–199 (2019).
73. M. Haas, M. P. Rastaldi, F. C. Fervenza, Histologic classification of glomerular diseases: Clinicopathologic correlations, limitations exposed by validation studies, and suggestions for modification. *Kidney Int.* **85**, 779–793 (2014).
74. M. N. Möller *et al*., Detection and quantification of nitric oxide-derived oxidants in biological systems. *J. Biol. Chem.* **294**, 14776–14802 (2019).
75. B. C. Dickinson, Y. Tang, Z. Chang, C. J. Chang, A nuclear-localized fluorescent hydrogen peroxide probe for monitoring sirtuin-mediated oxidative stress responses in vivo. *Chem. Biol.* **18**, 943–948 (2011).
76. S. Palanisamy *et al*., In vitro and in vivo imaging of peroxynitrite by a ratiometric boronate-based fluorescent probe. *Biosens. Bioelectron.* **91**, 849–856 (2017).
77. L. M. Villa, E. Salas, V. M. Darley-Usmar, M. W. Radomski, S. Moncada, Peroxynitrite induces both vasodilatation and impaired vascular relaxation in the isolated perfused rat heart. *Proc. Natl. Acad. Sci. U.S.A.* **91**, 12383–12387 (1994).
78. C. Gerassimou *et al*., Regulation of the expression of soluble guanylyl cyclase by reactive oxygen species. *Br. J. Pharmacol.* **150**, 1084–1091 (2007).
79. G. L. Baumbach, C. D. Sigmund, F. M. Faraci, Structure of cerebral arterioles in mice deficient in expression of the gene for endothelial nitric oxide synthase. *Circ. Res.* **95**, 822–829 (2004).
80. A. J. A. Leloup, C. E. Van Hove, S. De Moudt, G. W. De Keulenaer, P. Fransen, Ex vivo aortic stiffness in mice with different eNOS activity. *Am. J. Physiol. Heart Circ. Physiol.* **318**, H1233–H1244 (2020).
81. K. Numaguchi *et al*., Chronic inhibition of nitric oxide synthesis causes coronary microvascular remodeling in rats. *Hypertension* **26**, 957–962 (1995).
82. H. Ischiropoulos *et al*., Peroxynitrite-mediated tyrosine nitration catalyzed by superoxide dismutase. *Arch. Biochem. Biophys.* **298**, 431–437 (1992).
83. M. H. Zou, V. Ullrich, Peroxynitrite formed by simultaneous generation of nitric oxide and superoxide selectively inhibits bovine aortic prostacyclin synthase. *FEBS Lett.* **382**, 101–104 (1996).
84. P. Schmidt *et al*., Specific nitration at tyrosine 430 revealed by high resolution mass spectrometry as basis for redox regulation of bovine prostacyclin synthase. *J. Biol. Chem.* **278**, 12813–12819 (2003).
85. L. A. MacMillan-Crow, J. P. Crow, J. D. Kerby, J. S. Beckman, J. A. Thompson, Nitration and inactivation of manganese superoxide dismutase in chronic rejection of human renal allografts. *Proc. Natl. Acad. Sci. U.S.A.* **93**, 11853–11858 (1996).
86. V. Demicheli, D. M. Moreno, R. Radi, Human Mn-superoxide dismutase inactivation by peroxynitrite: A paradigm of metal-catalyzed tyrosine nitration in vitro and in vivo. *Metallomics* **10**, 679–695 (2018).
87. M. R. Siddiqui *et al*., Caveolin-1-eNOS signaling promotes p190RhoGAP-A nitration and endothelial permeability. *J. Cell Biol.* **193**, 841–850 (2011).
88. Y. Y. Zhao *et al*., Persistent eNOS activation secondary to caveolin-1 deficiency induces pulmonary hypertension in mice and humans through PKG nitration. *J. Clin. Invest.* **119**, 2009–2018 (2009).
89. P. A. Erwin, D. A. Mitchell, J. Sartoretto, M. A. Marletta, T. Michel, Subcellular targeting and differential S-nitrosylation of endothelial nitric-oxide synthase. *J. Biol. Chem.* **281**, 151–157 (2006).
90. C. Batthyány *et al*., Tyrosine-nitrated proteins: Proteomic and bioanalytical aspects. *Antioxid. Redox Signal.* **26**, 313–328 (2017).
91. A. A. Turanov, D. Su, V. N. Gladyshev, Characterization of alternative cytosolic forms and cellular targets of mouse mitochondrial thioredoxin reductase. *J. Biol. Chem.* **281**, 22953–22963 (2006).
92. S. R. Lee *et al*., Molecular cloning and characterization of a mitochondrial selenocysteine-containing thioredoxin reductase from rat liver. *J. Biol. Chem.* **274**, 4722–4734 (1999).
93. S. Watabe *et al*., Mitochondrial thioredoxin reductase in bovine adrenal cortex its purification, properties, nucleotide/amino acid sequences, and identification of selenocysteine. *Eur. J. Biochem.* **264**, 74–84 (1999).
94. L. Zhong, E. S. Arnér, A. Holmgren, Structure and mechanism of mammalian thioredoxin reductase: The active site is a redox-active selenolthiol/selenenylsulfide formed from the conserved cysteine-selenocysteine sequence. *Proc. Natl. Acad. Sci. U.S.A.* **97**, 5854–5859 (2000).

95. D. A. Drechsel, M. Patel, Respiration-dependent H2O2 removal in brain mitochondria via the thioredoxin/peroxiredoxin system. *J. Biol. Chem.* **285**, 27850–27858 (2010).
96. B. A. Stanley *et al*., Thioredoxin reductase-2 is essential for keeping low levels of H(2)O(2) emission from isolated heart mitochondria. *J. Biol. Chem.* **286**, 33669–33677 (2011).
97. X. Zhou, D. Yuan, M. Wang, P. He, H2O2-induced endothelial NO production contributes to vascular cell apoptosis and increased permeability in rat venules. *Am. J. Physiol. Heart Circ. Physiol.* **304**, H82–H93 (2013).
98. X. Zhou, Y. Qian, D. Yuan, Q. Feng, P. He, H_2O_2-induced microvessel barrier dysfunction: The interplay between reactive oxygen species, nitric oxide, and peroxynitrite. *Physiol. Rep.* **7**, e14206 (2019).
99. A. E. Vercesi *et al*., Mitochondrial calcium transport and the redox nature of the calcium-induced membrane permeability transition. *Free Radic. Biol. Med.* **129**, 1–24 (2018).
100. E. Eroglu *et al*., Development of novel FP-based probes for live-cell imaging of nitric oxide dynamics. *Nat. Commun.* **7**, 10623 (2016).
101. G. Cheng *et al*., Detection of mitochondria-generated reactive oxygen species in cells using multiple probes and methods: Potentials, pitfalls, and the future. *J. Biol. Chem.* **293**, 10363–10380 (2018).
102. C. Johansson, C. H. Lillig, A. Holmgren, Human mitochondrial glutaredoxin reduces S-glutathionylated proteins with high affinity accepting electrons from either glutathione or thioredoxin reductase. *J. Biol. Chem.* **279**, 7537–7543 (2004).
103. M. S. Seo *et al*., Identification of a new type of mammalian peroxiredoxin that forms an intramolecular disulfide as a reaction intermediate. *J. Biol. Chem.* **275**, 20346–20354 (2000).
104. G. Ferrer-Sueta, L. Hannibal, I. Batinic-Haberle, R. Radi, Reduction of manganese porphyrins by flavoenzymes and submitochondrial particles: A catalytic cycle for the reduction of peroxynitrite. *Free Radic. Biol. Med.* **41**, 503–512 (2006).
105. V. Valez *et al*., peroxynitrite formation in nitric oxide-exposed submitochondrial particles: Detection, oxidative damage and catalytic removal by Mn-porphyrins. *Arch. Biochem. Biophys.* **529**, 45–54 (2013).
106. N. Subelzu, S. Bartesaghi, A. de Bem, R. Radi, "Oxidative inactivation of nitric oxide and peroxynitrite formation in the vasculature" in *Oxidative Stress: Diagnostics, Prevention, and Therapy*, M. Hepel, S. Andreescu, Eds. (Symposium Series, ACS Books, 2015), vol. 2, chap. 4, pp. 91–145.
107. Y. Wang *et al*., Ephrin-B2 controls VEGF-induced angiogenesis and lymphangiogenesis. *Nature* **465**, 483–486 (2010).